Instantaneous Complex Power Control of a Grid-Tied VSC Supplying a Constant Power Load

Jorge A. Solsona, *Senior Member, IEEE*, Sebastian Gomez Jorge, Andres E. Leon, *Senior Member, IEEE*, and Claudio A. Busada

***Abstract*—In this article, a nonlinear controller for a grid-tied voltage-source converter (VSC) supplying a constant power load is introduced. The control law combines a feedback loop and a feedforward compensator. The feedback loop strategy uses a feedback linearizing method for compensating nonlinearities appearing in the VSC model. The performance in the presence of changes between two different values of constant power is improved by including a fast feedforward compensation. This compensator uses estimates of power load and its time derivative obtained from a nonlinear observer. The resultant strategy is validated via simulation and experimental tests. These experiments show that the proposed scheme performs in a very good way.**

***Index Terms*—Constant power load (CPL), instantaneous power, nonlinear control, nonlinear observer, voltage-source converter (VSC).**

I. Introduction

AT PRESENT, industrial equipment has evolved to include a lot of electronic components. Among others, power sources use voltage-source converters (VSCs) for modifying the input voltage level and waveform. In many applications, it is needed to convert currents and voltages from ac to dc and *vice versa*. Moreover, currently, when ac currents and voltages are changed in frequency, the input sinusoidal signal is changed to dc in a first stage, and in a second stage, dc waveform is changed to ac [1], [2].

It can be mentioned that in grid applications, the VSC is used for conforming different voltage and current sources with different kinds of waveforms. These sources are included as a part of a lot of equipment appearing in modern grid applications. Among others, it is possible to mention electric drives, static compensators, active power filters, and unified power conditioners. In addition, this converter can be found in electric vehicle applications and renewable energy sources, such as wind power and photovoltaic grid integration.

In these applications, the system performance depends on the control strategy used for controlling the electrical variables and for rejecting disturbance due to the electrical load variability. For these reasons, different control strategies, which can be found in the literature, have been proposed by many researchers. In some papers, nonlinear VSC dynamics is not considered and linear strategies are used [3]–[5]. Among others, feedback linearization, also called flatness, can be found in [6]–[8]; reduced-order generalized observers are used in [9]; and energy shaping is proposed in [10].

Many times, controllers are designed assuming that inductor currents and capacitor voltages are the state variables. However, it is possible to reformulate the model by using instantaneous power and energy as state variables. This representation is useful when a constant power load (CPL) is to be driven, since power balances appear in a natural way. In some papers, instantaneous power has been introduced for the description of the system (see, among others, [11]–[17]). It must be noted that in many applications, the load can be assumed to be a CPL [18]. It is well known that a VSC feeding a CPL is a highly nonlinear system [19].

In this article, a nonlinear control strategy is proposed for controlling the instantaneous complex power in a VSC feeding a CPL. This control strategy is based on a feedback linearizing controller combined with a feedforward compensator. This feedforward compensator is included for improving the disturbance rejection of the controller. In order to avoid including extra sensors, a nonlinear observer is designed for estimating the load and its time derivative values.

The rest of this article is organized as follows. Section II describes the system model as a function of the complex power and describes a compensation method for the effect of the dead time of the switches. In Section III, the proposed nonlinear control strategy is developed. Section IV summarizes the proposed strategy and described its implementation. Section V shows simulation and experimental results that validate the proposal. Finally, Section VI concludes this article.

II. System Model

The diagram of the VSC to be controlled is shown in Fig. 1. In the figure, the power taken by the load is P_L and is modeled as a controlled current source. The system of Fig. 1 is described

Manuscript received March 23, 2020; revised July 7, 2020; accepted August 16, 2020. Date of publication August 20, 2020; date of current version October 30, 2020. This work was supported in part by the Universidad Nacional del Sur, in part by the Consejo Nacional de Investigaciones Científicas y Técnicas, and in part by the Agencia Nacional de Promoción Científica y Tecnológica, Argentina. Recommended for publication by Associate Editor M. Ordonez. *(Corresponding author: Sebastian Gomez Jorge.)*

The authors are with the Instituto de Investigaciones en Ingeniería Eléctrica, Consejo Nacional de Investigaciones Científicas y Técnicas, Departamento de Ingeniería Eléctrica y de Computadoras, Universidad Nacional del Sur, 8000 Bahía Blanca, Argentina (e-mail: jsolsona@uns.edu.ar; sebastian.gomezjorge@uns.edu.ar; andreseleon@gmail.com; cbusada@uns.edu.ar).

Color versions of one or more of the figures in this article are available online at https://ieeexplore.ieee.org.

Digital Object Identifier 10.1109/TPEL.2020.3018396

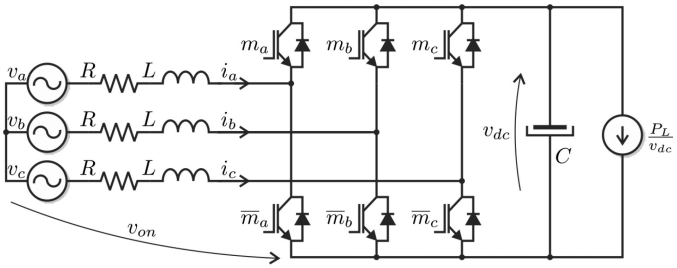

Fig. 1. Model of the VSC with a power load connected to the dc link.

by the following set of equations:

$$L\dot{i}_a = v_a - Ri_a - \sqrt{\rho E}m_a - v_{\text{on}} \tag{1}$$

$$L\dot{i}_b = v_b - Ri_b - \sqrt{\rho E}m_b - v_{\text{on}} \tag{2}$$

$$L\dot{i}_c = v_c - Ri_c - \sqrt{\rho E}m_c - v_{\text{on}} \tag{3}$$

$$v_{\text{on}} = -\sqrt{\rho E}(m_a + m_b + m_c)/3 \tag{4}$$

$$\dot{E} = \sqrt{\rho E}(i_a m_a + i_b m_b + i_c m_c) - P_L \tag{5}$$

where m_a, m_b, and m_c are the modulation indexes of each leg of the VSC, and $\rho = 2/C$. The capacitor dynamics is modeled in terms of its energy

$$E = \frac{1}{2}Cv_{\text{dc}}^2. \tag{6}$$

To reduce the number of equations and simplify the notation, we will transform this set of equations to a stationary $\alpha\beta$ reference frame and also use complex space vector notation. The power-invariant Clarke transform to the complex stationary reference frame is

$$\vec{f} = f_\alpha + jf_\beta = \sqrt{\frac{2}{3}}\left[f_a - 0.5f_b - 0.5f_c + j\frac{\sqrt{3}}{2}(f_b - f_c)\right] \tag{7}$$

where f_a, f_b, and f_c are arbitrary variables. Note that complex quantities are denoted with an over arrow. Applying (7) to (1)–(5), the system description results

$$L\dot{\vec{i}} = \vec{v} - R\vec{i} - \sqrt{\rho E}\vec{m} \tag{8}$$

$$\dot{E} = \sqrt{\rho E}\Re\{\vec{m}'\vec{i}\} - P_L \tag{9}$$

where $\vec{v} = v_\alpha + jv_\beta$, $\vec{i} = i_\alpha + ji_\beta$, and $\vec{m} = m_\alpha + jm_\beta$ are complex variables, representing the grid voltage, the grid current, and the modulation index. In addition, superscript $'$ stands for complex conjugate of a given variable.

A. Dead Time Disturbance and Grid Voltage Compensation

In order to avoid shoot through of the switches due to their turn-ON and turn-OFF times, the gate signals are usually modified to have a dead time. This dead time introduces an undesirable distortion in the grid current at the zero crossings of each of the phase currents. Although the dead time effect on shape of the gate signals is perfectly known, its effect on the shape of VSC voltages depends on zero crossings of the phase currents. To model this effect, the modulation index of each phase is divided as follows:

$$m_x = m_{rx} + m_{dx} \text{ with } x = a,\ b,\ \text{or } c \tag{10}$$

where m_{rx} is the reference modulation index, imposed by the controller (perfectly known), and m_{dx} is called disturbance modulation index, and it is imposed by the dead time and the instantaneous phase currents (unknown disturbance). Note that only reference modulation index m_{rx} is actually sent to the pulsewidth modulator (PWM) to generate the gate signals. Disturbance modulation index m_{dx} is defined here to model the effect that the turn-ON delay (imposed to the gate signals) has on the actual VSC phase voltages. Its average effect (over a PWM cycle) is approximated by

$$m_{dx} \simeq \frac{T_{\text{dt}}}{T_{\text{pwm}}}\text{sign}(i_x) \text{ with } x = a,\ b,\ \text{or } c \tag{11}$$

where T_{dt} is the dead time and T_{pwm} is the pulsewidth modulation period. Since these disturbances are square waves in phase with the grid currents, in complex variable [applying (7)], they become a positive-sequence fundamental frequency signal with harmonics. Through testing, it was found that for compensation purposes, it is enough to model its main harmonics (negative fifth and positive seventh); therefore, the following model is proposed for this signal:

$$\vec{m}_d = \vec{m}_{d1} + \vec{m}_{d5} + \vec{m}_{d7} \tag{12}$$

$$\dot{\vec{m}}_{d1} = j\omega\vec{m}_{d1} \tag{13}$$

$$\dot{\vec{m}}_{d5} = -j5\omega\vec{m}_{d5} \tag{14}$$

$$\dot{\vec{m}}_{d7} = j7\omega\vec{m}_{d7} \tag{15}$$

where $\vec{m}_{d1}$, $\vec{m}_{d5}$, and $\vec{m}_{d7}$ are, respectively, the fundamental, fifth, and seventh harmonic components of the disturbance modulation index.

To compensate the effect of this disturbance, we propose a feedforward compensation by adding its estimated value $\hat{\vec{m}}_d$ to the control modulation index. In addition, to compensate the effect of the grid voltage, its measured value will also be added through feedforward compensation. Therefore, the reference modulation index can be divided into a control term $\vec{m}_c$ and a feedforward compensation term:

$$\vec{m}_r = \vec{m}_c + \underbrace{\frac{\vec{v}}{\sqrt{\rho E}} - \hat{\vec{m}}_d}_{\text{feedforward}}. \tag{16}$$

Transforming (10) to complex variable and replacing $\vec{m}_r$ with (16), the complex modulation index applied to the system results in

$$\vec{m} = \vec{m}_r + \vec{m}_d = \vec{m}_c + \frac{\vec{v}}{\sqrt{\rho E}} + \vec{e}_d \tag{17}$$

where $\vec{e}_d = \vec{m}_d - \hat{\vec{m}}_d$. Replacing (17) in (8) and (9), the dynamics of the system with the feedforward compensation results in

$$L\dot{\vec{i}} = -R\vec{i} - \sqrt{\rho E}(\vec{m}_c + \vec{e}_d) \tag{18}$$

$$\dot{E} = \sqrt{\rho E}\Re\left\{(\vec{m}_c' + \frac{\vec{v}'}{\sqrt{\rho E}} + \vec{e}_d')i\right\} - P_L. \quad (19)$$

From the disturbance model (12)–(15) and (18), the following disturbance observer is proposed:

$$L\dot{\hat{\vec{i}}} = -R\hat{\vec{i}} - \sqrt{\rho E}\vec{m}_c + L\vec{h}_1\vec{e}_i \quad (20)$$

$$\dot{\hat{\vec{m}}}_{d1} = j\omega\hat{\vec{m}}_{d1} + \vec{h}_2\vec{e}_i \quad (21)$$

$$\dot{\hat{\vec{m}}}_{d5} = -j5\omega\hat{\vec{m}}_{d5} + \vec{h}_3\vec{e}_i \quad (22)$$

$$\dot{\hat{\vec{m}}}_{d7} = j7\omega\hat{\vec{m}}_{d7} + \vec{h}_4\vec{e}_i \quad (23)$$

$$\hat{\vec{m}}_d = \hat{\vec{m}}_{d1} + \hat{\vec{m}}_{d5} + \hat{\vec{m}}_{d7} \quad (24)$$

where $\vec{e}_i = \vec{i} - \hat{\vec{i}}$. Parameters $\vec{h}_1 \ldots \vec{h}_4$ are complex constants that determine the dynamic response of the observer. The error dynamics of this observer results in

$$\begin{bmatrix}\dot{\vec{e}}_i\\ \dot{\vec{e}}_{d1}\\ \dot{\vec{e}}_{d5}\\ \dot{\vec{e}}_{d7}\end{bmatrix} = \underbrace{\begin{bmatrix}-\vec{h}_1 - \frac{R}{L} & -\frac{\sqrt{\rho E}}{L} & -\frac{\sqrt{\rho E}}{L} & -\frac{\sqrt{\rho E}}{L}\\ -\vec{h}_2 & j\omega & 0 & 0\\ -\vec{h}_3 & 0 & -j5\omega & 0\\ -\vec{h}_4 & 0 & 0 & j7\omega\end{bmatrix}}_{A_d}\begin{bmatrix}\vec{e}_i\\ \vec{e}_{d1}\\ \vec{e}_{d5}\\ \vec{e}_{d7}\end{bmatrix} \quad (25)$$

where $\vec{e}_{d1} = \vec{m}_{d1} - \hat{\vec{m}}_{d1}$, $\vec{e}_{d5} = \vec{m}_{d5} - \hat{\vec{m}}_{d5}$, and $\vec{e}_{d7} = \vec{m}_{d7} - \hat{\vec{m}}_{d7}$. If E is kept almost constant at its reference value, the error dynamics will be linear. Then, the gains are chosen to place the eigenvalues of A_d (poles of the observer) to obtain the desired dynamic response using linear techniques, such as pole placement [20]. We will use this technique for all the linear controllers. Note that once the observer converges, $\vec{e}_d \to 0$ in (18) and (19), the dead time disturbance is effectively eliminated. As an additional feature, if the grid voltage cancelation is not perfect (for example, due to processing delay), the observer will also compensate the cancelation mismatch on the fundamental, fifth, and seventh harmonics.

B. System Model as a Function of the Complex Grid Power

Assuming that the grid voltage has a positive-sequence fundamental component with angular frequency ω plus harmonics, then this grid voltage can be modeled as

$$\vec{v} = \vec{v}_1 + \vec{v}_h \quad (26)$$

where

$$\dot{\vec{v}}_1 = j\omega\vec{v}_1 \quad (27)$$

and $\vec{v}_h$ contains all the harmonics. The fundamental and the main harmonic components of the grid voltage are obtained here using the frequency locked loop (FLL) proposed in [21]. If the grid current is controlled to be a positive-sequence pure sinusoidal signal with angular frequency ω, then we define the instantaneous fundamental complex grid power as

$$\vec{S}_1 = \vec{v}_1\vec{i}' = P_1 + jQ_1 \quad (28)$$

where P_1 and Q_1 are the instantaneous active and reactive powers, respectively. Differentiating (28) with respect to time, and replacing with (18) and (27), the system is described in terms of the grid power by

$$\dot{\vec{S}}_1 = \left(j\omega - \frac{R}{L}\right)\vec{S}_1 - \frac{\sqrt{\rho E}\vec{v}_1}{L}\vec{m}_c' - \frac{\vec{v}_1\sqrt{\rho E}}{L}\vec{e}_d' \quad (29)$$

$$\dot{E} = \frac{\sqrt{\rho E}}{|\vec{v}_1|^2}\Re\left\{\left(\vec{m}_c' + \frac{\vec{v}'}{\sqrt{\rho E}} + \vec{e}_d'\right)\vec{S}_1'\vec{v}_1\right\} - P_L \quad (30)$$

where (30) is obtained from (19) replacing $\vec{i} = \vec{S}_1'\vec{v}_1/|\vec{v}_1|^2$.

III. Nonlinear Control Strategy

Before proceeding to the linearization of the system, it is convenient to find a transformation to decouple the active and reactive grid powers. This step is not necessary to perform the linearization, but it is done here to obtain more compact equations and simpler notation.

A. Power Decoupling

To decouple the active and reactive grid powers, we define

$$\dot{\vec{S}}_1 = \vec{u} = u_p + ju_q \quad (31)$$

where $\vec{u}$ is an auxiliary control action that allows decoupled control of active and reactive powers. From this definition and (29), the control modulation index $\vec{m}_c$ that achieves this decoupling can be found as a function of $\vec{u}$ through

$$\vec{m}_c = -\frac{L\vec{v}_1}{\sqrt{\rho E}|\vec{v}_1|^2}\left[\vec{u}' + \left(\frac{R}{L} - j\omega\right)\vec{S}_1' + \frac{\vec{v}_1'\sqrt{\rho E}}{L}\vec{e}_d\right]. \quad (32)$$

Note that computing this equation requires knowledge of the disturbance error $\vec{e}_d$. However, if the disturbance observer is faster than the control loop, we can neglect this term when computing the control modulation index $\vec{m}_c$; therefore, we have

$$\vec{m}_c = -\frac{L\vec{v}_1}{\sqrt{\rho E}|\vec{v}_1|^2}\left[\vec{u}' + \left(\frac{R}{L} - j\omega\right)\vec{S}_1'\right]. \quad (33)$$

Replacing (33) in (30), the system written as a function of the new control variable results in

$$\dot{\vec{S}}_1 = \dot{P}_1 + j\dot{Q}_1 = u_p + ju_q \quad (34)$$

$$\dot{E} = P_1 - \frac{L(P_1u_p + Q_1u_q)}{|\vec{v}_1|^2} - \frac{R|\vec{S}_1|^2}{|\vec{v}_1|^2} - P_L + \Re\left\{\frac{\vec{S}_1'\vec{v}_1\sqrt{\rho E}}{|\vec{v}_1|^2}\vec{e}_d'\right\} + \Re\left\{\frac{\vec{v}_1\vec{v}_h'\vec{S}_1'}{|\vec{v}_1|^2}\right\}. \quad (35)$$

This last equation shows the well-known input output power balance of a system. The energy variation in the dc link is the grid input power (first term) minus the inductor energy variation (second term) minus resistive losses (third term) minus load power (fourth term). The fifth term of (35) appears due to neglecting the last term of (32) and can be neglected here for the same reason, since the disturbance observer is designed to be fast. The last term has zero mean value and shows that there will be harmonic content in the dc-link energy due to the effect

of the grid harmonics. For typical grid voltage harmonic distortion levels (<10%) and dc-link capacitor values, the harmonic frequency ripple voltage in the dc link is usually a few volts and can be neglected without significant performance impact.

The resulting system (34), (35) is still highly nonlinear, so we will define another change of variables to fully linearize it. In what follows, the last two terms of (35) will be assumed zero.

B. Complex Exact Feedback Linearization

System (34), (35) can be input–output linearized by choosing the instantaneous complex energy as the output variable. The real part of this energy is due to the active power transfer, while the imaginary part is due to the reactive power. The instantaneous complex energy is, therefore, defined as

$$\vec{z}_1 = \underbrace{\frac{1}{2}L\frac{|\vec{S}_1|^2}{|\vec{v}_1|^2} + E}_{z_{1p}} + jz_{1q} \tag{36}$$

where z_{1q} is the imaginary energy due to the reactive grid power and is defined through

$$\dot{z}_{1q} = Q_1. \tag{37}$$

The first time derivative of $\vec{z}_1$ results in

$$\dot{\vec{z}}_1 = \vec{z}_2 = \underbrace{P_1 - R\frac{|\vec{S}_1|^2}{|\vec{v}_1|^2} - P_L}_{z_{2p}} + j\underbrace{Q_1}_{z_{2q}} \tag{38}$$

where the real part of variable $\vec{z}_2$ is the rate of change in the system stored energy, while its imaginary part is the grid reactive power. Differentiating once more with respect to time, we obtain

$$\dot{\vec{z}}_2 = \vec{W} = \underbrace{u_p - \frac{2R(P_1u_p + Q_1u_q)}{|\vec{v}_1|^2} - \dot{P}_L}_{W_p} + j\underbrace{u_q}_{W_q} \tag{39}$$

where $\vec{W}$ is the complex control action of the fully linearized system

$$\dot{\vec{z}}_1 = \vec{z}_2 \tag{40}$$

$$\dot{\vec{z}}_2 = \vec{W}. \tag{41}$$

This system can be controlled using a linear controller. Once control action $\vec{W}$ is computed, auxiliary control action $\vec{u}$ of the decoupled system is computed from (39) through

$$\vec{u} = \frac{|\vec{v}_1|^2}{|\vec{v}_1|^2 - 2RP_1}\left(W_p + \dot{P}_L + \frac{2RQ_1W_q}{|\vec{v}_1|^2}\right) + jW_q. \tag{42}$$

Note that for computing $\vec{z}_2$ and recovering $\vec{u}$, we require knowledge of the load power and its time derivative. Instead of measuring these quantities, they will be estimated using an observer described in Section III-E.

Once auxiliary control action $\vec{u} = u_p + ju_q$ is obtained from (42), the control modulation index $\vec{m}_c$ is computed through (33), and then, the reference modulation index $\vec{m}_r$ that is sent to the PWM is computed through (16).

C. Linear Law for the Linearized System

Since the real stored energy of the system is z_{1p} and the reactive power is z_{2q} and these variables are decoupled, we will design two control loops. For the energy control loop, a full-state feedback with integral term is proposed

$$W_p = -k_1(z_{1p} - z_{1p}^*) - k_2(z_{2p} - z_{2p}^*) - k_3y_p \tag{43}$$

$$\dot{y}_p = z_{1p} - z_{1p}^* \tag{44}$$

where k_1, k_2, and k_3 are feedback gains, and z_{1p}^* and z_{2p}^* are references, which will be defined in the next section. Combining (43) and (44) with the real part of the linearized system (40), (41), the closed-loop dynamics of the energy control loop results in

$$\begin{bmatrix}\dot{z}_{1p}\\ \dot{z}_{2p}\\ \dot{y}_p\end{bmatrix} = \underbrace{\begin{bmatrix}0 & 1 & 0\\ -k_1 & -k_2 & -k_3\\ 1 & 0 & 0\end{bmatrix}}_{A_p}\begin{bmatrix}z_{1p}\\ z_{2p}\\ y_p\end{bmatrix} + \begin{bmatrix}0 & 0\\ k_1 & k_2\\ -k_1 & 0\end{bmatrix}\begin{bmatrix}z_{1p}^*\\ z_{2p}^*\end{bmatrix} \tag{45}$$

where the gains are chosen to place the eigenvalues of A_p (closed-loop poles) to obtain the desired dynamic response. Note that this loop must be slower than the disturbance observer loop.

For the reactive power control loop, full-state feedback with an integral term is also proposed

$$W_q = -k_4(Q_1 - Q_1^*) - k_5y_q + \dot{Q}_1^* \tag{46}$$

$$\dot{y}_q = Q_1 - Q_1^* \tag{47}$$

where k_4 and k_5 are feedback gains and Q_1^* is an arbitrary reactive power reference. Since this reference is internally generated by the controller, we can perform trajectory tracking including its first time derivative, as seen in (46). Combining (46) and (47) with the imaginary part of (41), the closed-loop dynamics of the reactive power loop results in

$$\begin{bmatrix}\dot{e}_q\\ \dot{y}_q\end{bmatrix} = \underbrace{\begin{bmatrix}-k_4 & -k_5\\ 1 & 0\end{bmatrix}}_{A_q}\begin{bmatrix}e_q\\ y_q\end{bmatrix} \tag{48}$$

where $e_q = Q_1 - Q_1^*$ is the tracking error, and the gains are chosen to place the eigenvalues of A_q (closed-loop poles) to obtain the desired dynamic response. Note that this loop must also be slower than the disturbance observer loop.

D. Design of the Energy Control References

From the definition of z_{1p} in (36), the energy reference z_{1p}^* is computed through

$$z_{1p}^* = \frac{1}{2}L\frac{P_1^{*2} + Q_1^{*2}}{|\vec{v}_1|^2} + E^* \tag{49}$$

where $E^* = \frac{1}{2}Cv_{\text{dc}}^{*\,2}$, with v_{dc}^* being the dc-link reference voltage. Q_1^* is the reactive power reference, which can be set arbitrarily, and P_1^* is the active power reference. In order to find P_1^*, we will use the fact that in the steady state, $\dot{z}_{1p} = z_{2p} = 0$, since power balance must be reached. Then, replacing P_1 and

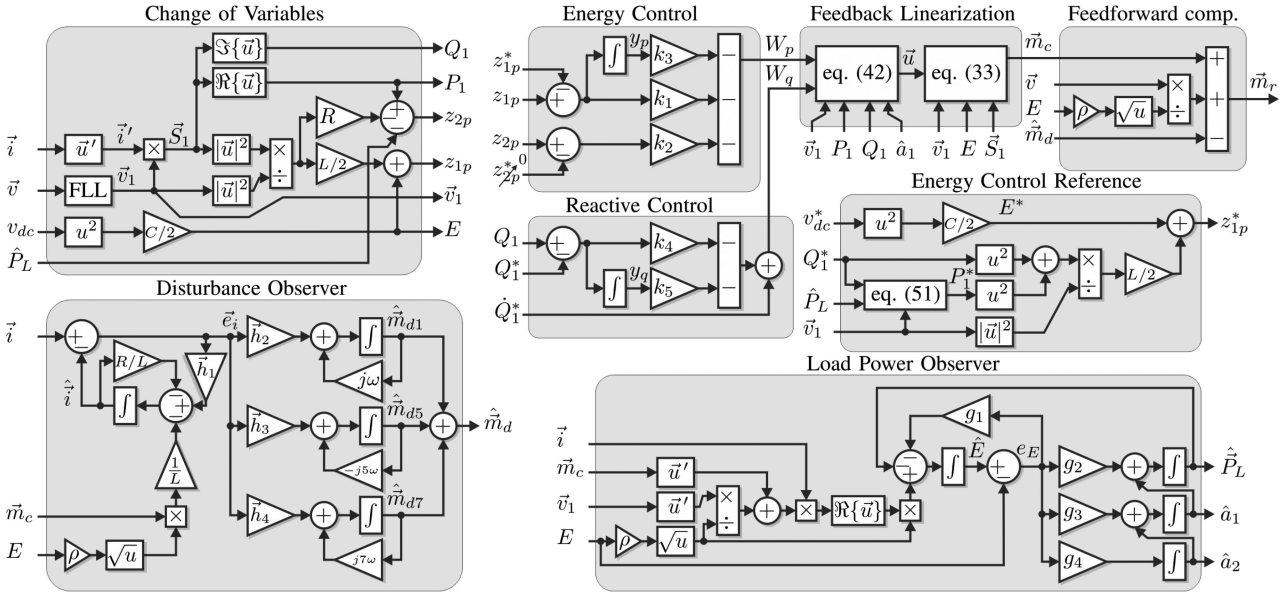

Fig. 2. Controller structure block diagram.

Q_1 in (38) by P_1^* and Q_1^* and equating to zero, we have the following Bhaskara equation:

$$0 = P_1^* - R\frac{P_1^{*2} + Q_1^{*2}}{|\vec{v}_1|^2} - P_L \tag{50}$$

from which the active power reference results in

$$P_1^* = \frac{|\vec{v}_1|^2 - \sqrt{|\vec{v}_1|^4 - 4R(|\vec{v}_1|^2 P_L + RQ_1^{*2})}}{2R}. \tag{51}$$

Since in the steady state, $z_{2p} = 0$, we will set its reference to $z_{2p}^* = 0$.

E. Load Power Observer

In order to design an observer for the load power, we must first define a model for the dynamics of this power. In most cases, assuming that the load power is constant works well enough. However, if the load changes slowly between two levels, it is better to include higher order time derivatives. For these cases, we will assume the following model:

$$\dot{P}_L = a_1 \tag{52}$$

$$\dot{a}_1 = \ddot{P}_L = a_2 \tag{53}$$

$$\dot{a}_2 = \dddot{P}_L = 0. \tag{54}$$

From this model and (19), assuming $\vec{e}_d \to 0$, the following observer is proposed:

$$\dot{\hat{E}} = \sqrt{\rho E}\Re\left\{\left(\vec{m}_c' + \frac{\vec{v}'}{\sqrt{\rho E}}\right)\vec{i}\right\} - \hat{P}_L + g_1 e_E \tag{55}$$

$$\dot{\hat{P}}_L = \hat{a}_1 + g_2 e_E \tag{56}$$

$$\dot{\hat{a}}_1 = \hat{a}_2 + g_3 e_E \tag{57}$$

$$\dot{\hat{a}}_2 = g_4 e_E \tag{58}$$

where $e_E = E - \hat{E}$. Defining error signals $e_{P_L} = P_L - \hat{P}_L$, $e_{a_1} = a_1 - \hat{a}_1$, and $e_{a_2} = a_2 - \hat{a}_2$, the error dynamics for this observer results in

$$\begin{bmatrix} \dot{e}_E \\ \dot{e}_{P_L} \\ \dot{e}_{a_1} \\ \dot{e}_{a_2} \end{bmatrix} = \underbrace{\begin{bmatrix} -g_1 & -1 & 0 & 0 \\ -g_2 & 0 & 1 & 0 \\ -g_3 & 0 & 0 & 1 \\ -g_4 & 0 & 0 & 0 \end{bmatrix}}_{A_{P_L}} \begin{bmatrix} e_E \\ e_{P_L} \\ e_{a_1} \\ e_{a_2} \end{bmatrix} \tag{59}$$

where the gains are chosen to place the eigenvalues of A_{P_L} (poles of the observer) to obtain the desired dynamic response. It must be noted that since we have assumed that $\vec{e}_d \to 0$, the dynamic response of this observer must be slower than that of the disturbance observer of Section II-A, but faster than the one of the energy control loop of Section III-C.

IV. Controller Structure Summary

Fig. 2 summarizes the proposed controller structure in a block diagram in complex variable (Clarke transform not shown). The block "Change of Variables" uses measured signals $\vec{v}$, $\vec{i}$, and $v_{\rm dc}$ to implement (6), (28), and the real parts of (36) and (38). Here, the measurement of load power P_L is avoided using instead its estimated value $\hat{P}_L$. In addition, the fundamental component of the grid voltage $\hat{v}_1$ is obtained using the FLL proposed in [21]. The block "Disturbance Observer" implements (20)–(24), "Energy Control" implements (43) and (44), "Reactive Control" implements (46) and (47), and "Load Power Observer" implements (55)–(58). The block "Feedback Linearization" implements (33) and (42), where $\dot{P}_L$ is replaced by its estimate $\hat{a}_1$. "Energy Control Reference" implements (49) and (51), where P_L is replaced by its estimate $\hat{P}_L$. Finally, "Feedforward Comp." implements (16). The output of this block is then transformed to the abc frame using the inverse Clarke transform to obtain

reference modulation indexes m_{ra}, m_{rb}, and m_{rc}, which are sent to the PWM to generate the gate signals.

V. Simulation and Experimental Results

In this section, simulation and experimental results are presented. For both cases, the parameters of the VSC were $L = 4.06$ mH, $R = 0.542\,\Omega$, and $C = 470\,\mu$F. The controller gains for the energy control loop were chosen to obtain a settling time of 50 ms ($k_1 = 2.96 \times 10^5$, $k_2 = 1.01 \times 10^3$, and $k_3 = 19.456 \times 10^6$) and for the reactive power control loop to obtain a settling time of 5 ms ($k_4 = 1.84 \times 10^3$ and $k_5 = 1.693 \times 10^6$). The disturbance observer gains were chosen to obtain a settling time of less than 4 ms ($h_1 = 14.23 \times 10^3$, $h_2 = -228.3 - j17.95$, $h_3 = -222.2 - j166.8$, and $h_4 = -268.9 + j162.8$), and the load power observer gains to obtain a settling time of approximately 25 ms ($g_1 = 620.87$, $g_2 = -19.27 \times 10^4$, $g_3 = -29.85 \times 10^6$, and $g_4 = -23.12 \times 10^8$).

A. Simulation Results

The system of Fig. 1 was simulated, including PWM (20 kHz) and dead time (1 μs), using the controller described in Fig. 2. In order to emulate the voltage level of the three-phase step-down isolation transformer used in the experimental prototype of the next section, the grid voltage was set to 90.5 Vrms and 50 Hz with harmonics -5 (1.33%), $+7$ (0.5%), -11 (0.5%), and +13 (0.3%), with total harmonic distortion (THD) $= 1.54\%$.

Fig. 3 shows the simulation results. The dc link starts at 300 V, as shown in Fig. 3(d), with no load connected, and draining no current from the grid, as shown in Fig. 3(a). The grid active power reference P_1^* and the actual grid active power P_1 are zero, as shown in Fig. 3(b), as well as the reactive power reference Q_1^* and actual grid reactive power Q_1, which are shown in Fig. 3(c). At $t = 20$ ms, the reactive power reference is increased from 0 to 1410 var within 10 ms, following a soft profile. As a result, the grid current increases to 5.2 Arms, which, in turn, results in an increase in the reference active power and actual active powers, to cover the resistive losses. The dc-link voltage transient due to this reactive power increase is negligible. At $t = 105$ ms, a CPL is connected to the dc link and its power is increased from 0 to 1620 W within 50 ms, following a soft profile. As can be seen, the grid reference active power and actual grid active power transient stabilize approximately 25 ms after the load has reached its steady-state power, matching the load observer settling time. As a result, the grid current increases to 8.2 Arms. There is also a small transient in the dc-link voltage that lasts until the load observer reaches the steady state. At $t = 330$ ms, the reactive power is reduced to 0. This decreases the grid current and the active power drained from the grid, due to the reduction in resistive losses. Finally, at $t = 405$ ms, the CPL power is decreased to zero, which results in similar transients as when it was connected.

B. Effect of the Disturbance Observer

To highlight the effect of the disturbance observer, the previous simulation was repeated with the disturbance observer disabled (setting $\hat{\vec{m}}_d = 0$). Fig. 4 shows phase "a" grid currents for both cases. Since the benefits of the observer are more obvious at low currents, a time frame when only reactive power is being transferred (between $t = 80$ ms and $t = 100$ ms) is shown. In both cases, the THD is computed up to the 50th harmonic (2500 Hz). Fig. 4(a) shows the results with the observer enabled, where the current has a THD $= 0.83\%$, while Fig. 4(b) shows the results with the observer disabled, resulting in a THD $= 3.26\%$. The significantly larger distortion without the observer justifies its inclusion in the design.

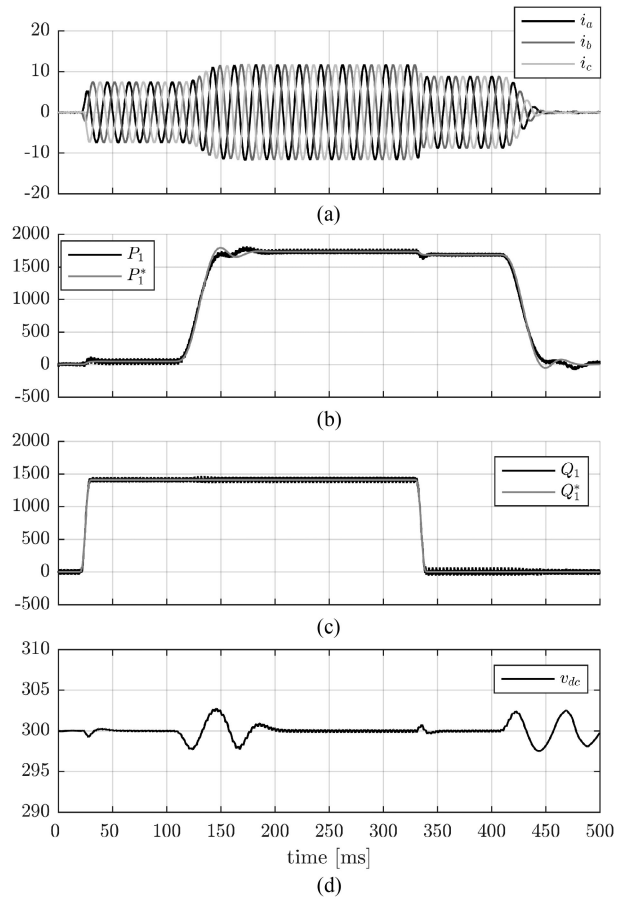

Fig. 3. Simulation results. (a) Grid phase currents [A]. (b) Grid active power reference and actual grid active power [W]. (c) Grid reactive power reference and actual grid reactive power [var]. (d) DC-link capacitor voltage [V].

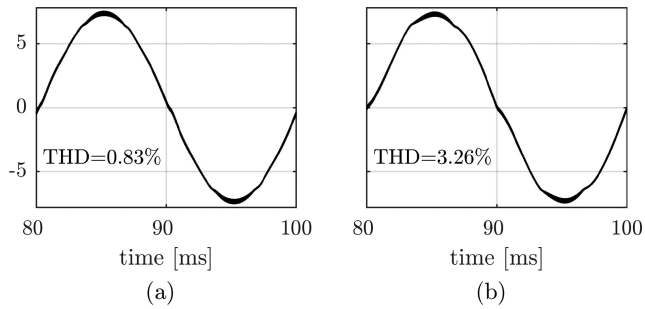

Fig. 4. Disturbance observer effect comparison. (a) With disturbance observer enabled. (b) Without disturbance observer ($\hat{\vec{m}}_d = 0$).

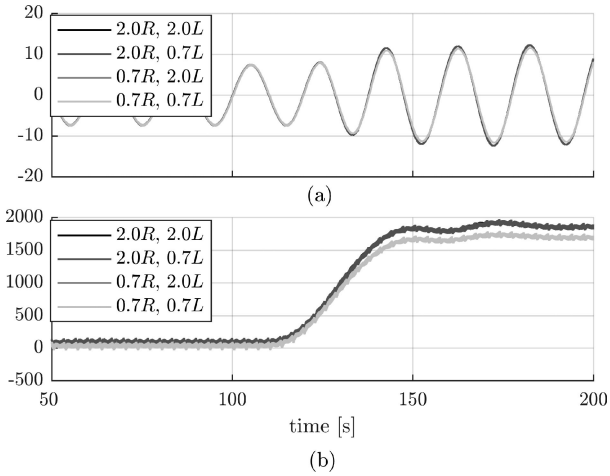

Fig. 5. Robustness simulation results. (a) Grid phase "a" currents [A]. (b) Grid active powers [W].

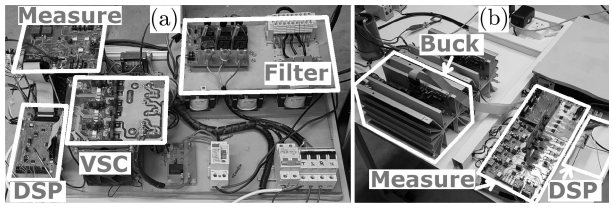

Fig. 6. Experimental setup. (a) VSC. (b) Buck converter (CPL).

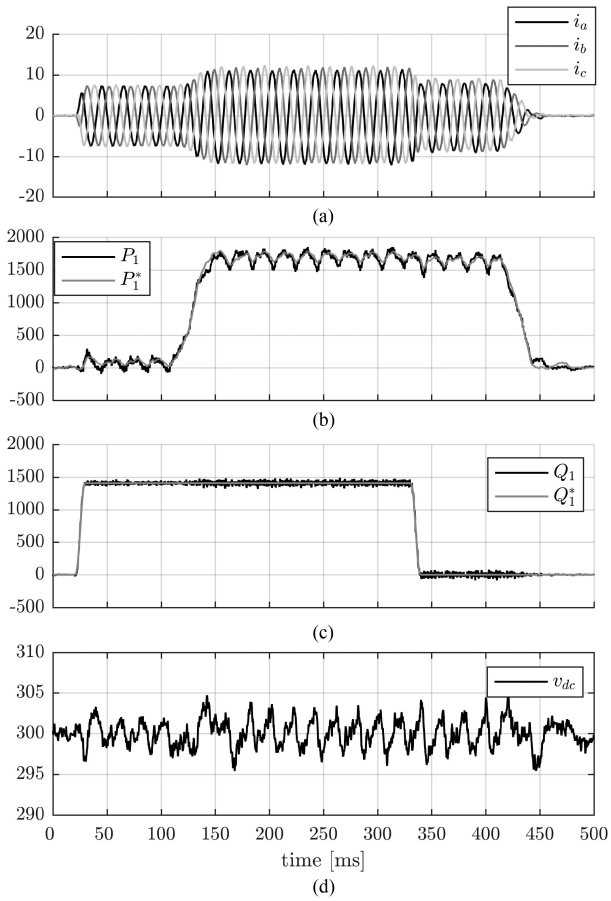

Fig. 7. Experimental results. (a) Grid phase currents [A]. (b) Grid active power reference and actual grid active power [W]. (c) Grid reactive power reference and actual grid reactive power [var]. (d) DC-link capacitor voltage [V].

C. Robustness

To verify the robustness of the proposal to variations of the parameters of the RL coupling filter, the simulations of Section V-A were repeated (using the same gain values) for a +100%, -30% variation of R and L around their nominal values. Fig. 5(a) shows phase "a" currents and Fig. 5(b) the active powers for the resulting four cases. A zoom around 50–200 ms is shown to verify if there is any significant transient response differences. As can be seen in the figure, the transient response is almost unaffected, and only a small increase in active power is noticeable (consistent with the increase of resistance). These results show the stability of the closed-loop system to a large parametric variation.

D. Experimental Results

The experimental results were obtained using a VSC built using IRG4PH50UD insulated-gate bipolar transistors (IGBTs). These IGBTs are controlled through a TMS320F28335 TI digital signal processor (DSP), with a sampling and PWM time of 50 μs. The dead time of the switches was set to 1 μs. To emulate the CPL, a buck converter was connected as load at the dc link, and its load profile was controlled using a DSP. The experimental setup is shown in Fig. 6. The VSC of Fig. 1 is shown in Fig. 6(a), and the CPL in Fig. 6(b). The VSC is connected to the grid through a three-phase step-down isolation transformer (not shown in the figure). The output voltage of this transformer is considered the grid voltage for the purposes of the experiment and has 90.5 Vrms with 50 Hz and THD $= 1.7\%$.

Fig. 7 shows the experimental results. The grid phase currents shown in Fig. 7(a) were obtained from the oscilloscope set to high-resolution mode. The active and reactive powers and the dc-link voltage were captured from the DSP memory and were sampled with a decimation of 2 (one sample every 100 μs). Here, the load profile and the reactive power profile were the same as in the simulations. As can be seen, the results are very similar. There is, however, some low-frequency ripple in the active power, which is also present on the dc-link voltage and results in some imbalance in the grid currents. This ripple is mainly caused by the grid voltage measurement sensors, which have a dc offset that is difficult to eliminate. For future tests, a better sensor will be used. Nevertheless, the distortion levels of the currents are acceptable, with a THD $= 2\%$ when both active and reactive grid powers are present (grid current 8.16 Arms).

Fig. 8 shows oscilloscope captures of phase a voltage and current for different power conditions. Fig. 8(a) shows a time frame when only reactive power is being injected to the grid. As can be seen, the current is lagging the voltage by 90°. Fig. 8(b) shows a time frame when both active and reactive powers are present in almost the same proportions, which results in the

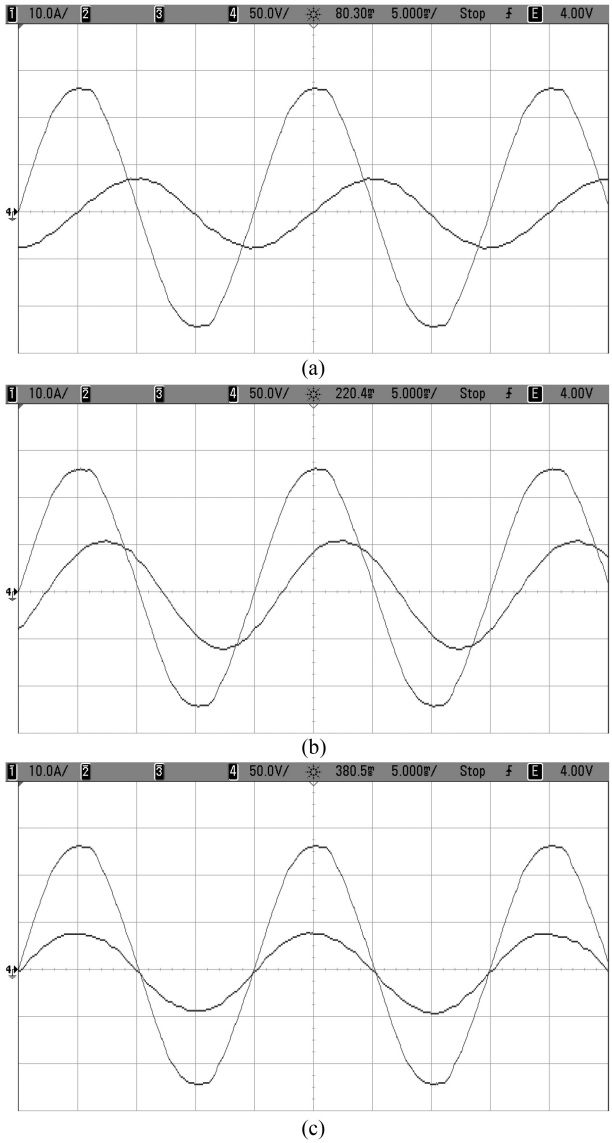

Fig. 8. Experimental results. Phase a grid voltage (50 V/div) and current (10 A/div) for (a) reactive power injection, (b) active and reactive power injection, and (c) active power injection.

current lagging approximately 45°. Finally, Fig. 8(c) shows a time frame when only active power is drained from the grid, and the current and phase voltage are in phase. These figures also show the low distortion level of the phase currents.

Both the simulations and experimental results shown in this section validate the proposed control strategy.

VI. Conclusion

This article proposes to model the VSC as a function of the grid power. Then, using this model, a feedback linearization strategy is designed. This allows the design of linear controllers, with known dynamic responses, to control the nonlinear system. The proposed feedback linearization strategy requires knowledge of the load power and its time derivatives, so an observer is proposed to estimate those. The proposed controller and observer are simulated and tested experimentally, and the results obtained validate the proposal.

References

[1] M. P. Kazmierkowski and L. Malesani, "Current control techniques for three-phase voltage-source PWM converters: A survey," *IEEE Trans. Ind. Electron.*, vol. 45, no. 5, pp. 691–703, Oct. 1998.

[2] R. Shah, J. C. Sánchez, R. Preece, and M. Barnes, "Stability and control of mixed ACDC systems with VSC-HVDC: A review," *IET Gener., Transmiss. Distrib.*, vol. 12, no. 10, pp. 2207–2219, May 2018.

[3] A. Doria-Cerezo and M. Bodson, "Design of controllers for electrical power systems using a complex root locus method," *IEEE Trans. Ind. Electron.*, vol. 63, no. 6, pp. 3706–3716, Jun. 2016.

[4] A. Doria-Cerezo, F. M. Serra, and M. Bodson, "Complex-based controller for a three-phase inverter with an *LCL* filter connected to unbalanced grids," *IEEE Trans. Power Electron.*, vol. 34, no. 4, pp. 3899–3909, Apr. 2019.

[5] S. Golestan, J. M. Guerrero, J. C. Vasquez, and A. M. Abusorrah, "Modeling and tuning of adaptive complex current controller for three-phase grid-interfaced power converters," in *Proc. IEEE Int. Conf. Environ. Elect. Eng. IEEE Ind. Commercial Power Syst. Eur.*, Jun. 2019, pp. 1–6.

[6] A. K. Pati and N. C. Sahoo, "Power quality improvement by feedback linearization control of grid connected three phase boost inverter," in *Proc. IEEE Power, Commun. Inf. Technol. Conf.*, Oct. 2015, pp. 599–604.

[7] A. Houari, H. Renaudineau, J.-P. Martin, S. Pierfederici, and F. Meibody-Tabar, "Flatness-based control of three-phase inverter with output *LC* filter" *IEEE Trans. Ind. Electron.*, vol. 59, no. 7, pp. 2890–2897, Jul. 2012.

[8] M. Kissaoui, A. A. R. A. Tahir, A. Abouloifa, F. Z. Chaoui, Y. Abouelmahjoub, and F. Giri, "Output-feedback nonlinear adaptive control strategy of three-phase AC/DC boost power converter for on-line UPS systems," *IFAC-PapersOnLine*, vol. 49, no. 13, pp. 324–329, 2016.

[9] S. Zhang, J. Zhao, Z. Zhao, K. Liu, P. Wang, and B. Yang, "Decoupled current controller based on reduced order generalized integrator for three-phase grid-connected VSCs in distributed system," *Energies*, vol. 12, no. 12, Jun. 2019, Art. no. 2426.

[10] C. Albea, F. Gordillo, and C. Canudas-De-Wit, "Adaptive control design for a boost inverter," *Control Eng. Pract.*, vol. 19, no. 1, pp. 32–44, Jan. 2011.

[11] M. Monfared, H. Rastegar, and H. M. Kojabadi, "High performance direct instantaneous power control of PWM rectifiers," *Energy Convers. Manage.*, vol. 51, no. 5, pp. 947–954, May 2010.

[12] E. Tedeschi, P. Tenti, and P. Mattavelli, "Cooperative operation of active power filters by instantaneous complex power control," in *Proc. 7th Int. Conf. Power Electron. Drive Syst.*, Nov. 2007, pp. 555–561.

[13] A. Lorduy, A. Lazaro, C. Fernandez, I. Quesada, and A. Barrado, "Novel simplified controller for three phase grid connected inverter based on instantaneous complex power," in *Proc. 24th Annu. IEEE Appl. Power Electron. Conf. Expo.*, Feb. 2009, pp. 1306–1312.

[14] Y. Beck, N. Calamaro, and D. Shmilovitz, "A review study of instantaneous electric energy transport theories and their novel implementations," *Renewable Sustain. Energy Rev.*, vol. 57, pp. 1428–1439, May 2016.

[15] W. Gil, O. D. Montoya, and A. Garces, "Direct power control of electrical energy storage systems: A passivity-based PI approach," *Electr. Power Syst. Res.*, vol. 175, 2019, Art. no. 105885.

[16] Y. Suh, V. Tijeras, and T. A. Lipo, "A nonlinear control of the instantaneous power in DQ synchronous frame for PWM AC/DC converter under generalized unbalanced operating conditions," in *Proc. 37th IEEE Ind. Appl. Soc. Annu. Meeting*, 2002,vol. 2, pp. 1189–1196,.

[17] D. L. Milanez and M. S. Miskulim, "The instantaneous complex power applied to three-phase machines," in *Proc. 28th IEEE Ind. Appl. Soc. Annu. Meeting*, 1993, pp. 171–176.

[18] E. Hossain, R. Perez, A. Nasiri, and S. Padmanaban, "A comprehensive review on constant power loads compensation techniques," *IEEE Access*, vol. 6, pp. 33285–33305, 2018.

[19] A. E. Leon, J. A. Solsona, and M. I. Valla, "Exponentially convergent estimator to improve performance of voltage source converters," *IET Power Electron.*, vol. 3, no. 5, pp. 668–680, 2010.

[20] R. J. Vaccaro, "Digital control: A state space approach [BOOKSHELF]," *IEEE Control Syst.*, New York, NY, USA: McGraw-Hill, vol. 16, no. 1, p. 90, Feb. 1995.

[21] S. G. Jorge, C. A. Busada, and J. A. Solsona, "Frequency adaptive discrete filter for grid synchronization under distorted voltages," *IEEE Trans. Power Electron.*, vol. 27, no. 8, pp. 3584–3594, Aug. 2012.

Jorge A. Solsona (Senior Member, IEEE) received the Electronics Engineer and Ph.D. degrees from the Universidad Nacional de La Plata, La Plata, Argentina, in 1986 and 1995, respectively.

He is currently a Professor with the Departamento de Ingeniería Electrica y de Computadoras, Instituto de Investigaciones en Ingeniería Eléctrica "Alfredo C. Desages," Universidad Nacional del Sur, Bahia Blanca, Argentina, where he is also with the Consejo Nacional de Investigaciones Científicas y Técnicas. He is involved in teaching and research on control theory and its applications to electromechanical systems.

Sebastian Gomez Jorge received the Electronics Engineer, M.S., and Ph.D. degrees from the Universidad Nacional del Sur, Bahía Blanca, Argentina, in 2006, 2009, and 2011, respectively.

He is currently with the Consejo Nacional de Investigaciones Científicas y Técnicas and the Instituto de Investigaciones en Ingeniería Eléctrica "Alfredo C. Desages," and with the Departamento de Ingeniería Eléctrica y de Computadoras, Universidad Nacional del Sur, where he is a Graduate Teaching Assistant.

Andres E. Leon (Senior Member, IEEE) received the degree in electrical engineering from the Universidad Nacional del Comahue, Neuquén, Argentina, in 2005, and the doctoral degree in control systems from the Universidad Nacional del Sur, Bahía Blanca, Argentina, in 2011.

Since 2012, he has been a Researcher with the National Scientific and Technical Research Council. He is currently working with the Research Institute of Electrical Engineering "Alfredo Desages," Universidad Nacional del Sur. His research interests include power system control and wind energy conversion systems.

Dr. Leon is an Associate Editor of the IEEE TRANSACTIONS ON SUSTAINABLE ENERGY.

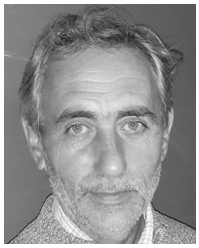

Claudio A. Busada was born in Bahía Blanca, Argentina, on March 13, 1962. He received the degree in electrical engineering and the Ph.D. degree in control systems from the Universidad Nacional del Sur, Bahía Blanca, in 1989 and 2004, respectively.

From 1988 to 2004, he was with the Mechanic and Electrical Department, City of Bahía Blanca. Since 1989, he has been with the Departamento de Ingeniería Eléctrica y de Computadoras, Universidad Nacional del Sur, where he is currently a Professor. He is a Researcher with the Instituto de Investigaciones en Ingeniería Eléctrica "Alfredo C. Desages," Universidad Nacional del Sur. His research interests include power electronics, rotating machinery, active filters, automatic control, and integration of distributed energy systems.